Relationships between crater and sputtered material characteristics in large gas cluster sputtering of polymers: Results from molecular dynamics simulations

Arnaud Delcorte, Konstantin Moshkunov, and Mathieu Debongnie

Citation: Journal of Vacuum Science & Technology B, Nanotechnology and Microelectronics: Materials, Processing, Measurement, and Phenomena **36**, 03F109 (2018);

View online: https://doi.org/10.1116/1.5012981

View Table of Contents: http://avs.scitation.org/toc/jvb/36/3

Published by the American Vacuum Society

Relationships between crater and sputtered material characteristics in large gas cluster sputtering of polymers: Results from molecular dynamics simulations

Arnaud Delcorte,[a] Konstantin Moshkunov, and Mathieu Debongnie
Institute of Condensed Matter and Nanosciences—Bio and Soft Matter (IMCN/BSMA), Université Catholique de Louvain, 1 Place Louis Pasteur, B-1348 Louvain-la-Neuve, Belgium

(Received 9 November 2017; accepted 22 January 2018; published 13 February 2018)

This molecular dynamics study focuses on the relationships between the sputtered volume and the crater size and shape as a function of scaled energy, upon a 45° incidence of $(Ar)_n$ and $(CH_4)_n$ clusters on an amorphous solid made of 1.4 kDa polymers $[CH_3\text{-}(CH_2)_{97}\text{-}CH_3]$. The cluster sizes were in the range of 10–10^4 and their kinetic energies, between 2.5 and 15 keV. The craters were satisfactorily approximated by semiellipsoids. First, our results show that the crater shape is a complex function of the projectile composition, number of constituents (nuclearity), and energy. This dependence can be presented as a single "universal" curve by plotting the crater volume, scaled by the projectile nuclearity or mass, versus the projectile energy scaled in the same way. Second, the ratio of the sputter yield volume Y_v over the crater volume V varies monotonically with the scaled energy, so that large impact craters are still formed under 0.025 eV/amu bombardment with almost no ejection, but only material displacement on the surface. While the sputtered material originates mostly from the top third of the crater at high scaled energy, the ejection is limited to surface molecules at low energy. This implies that large, slow clusters in addition to softer emission should provide more surface sensitivity for cluster-based molecular analysis. Finally, the relation between the craters and sputtering for ultrathin layers (2–15 nm) on a rigid substrate indicates that a maximum of sputtering efficiency is reached for 4 nm films in the case of 10 keV Ar_{3000} projectiles at 45° incidence. *Published by the AVS.* https://doi.org/10.1116/1.5012981

I. INTRODUCTION

Large argon clusters have become the projectiles of choice for soft sputtering of fragile organic materials in secondary ion mass spectrometry (SIMS). Because their kiloelectronvolt translational energy is distributed over a large number of atoms (n), the energy per atom E/n is of the order of electronvolts, i.e., equivalent or even inferior to the energy of molecular bonds. In this energy range and below, large clusters can still emit intact target molecules upon an impact and the fragmentation is minimal. Detailed measurements of the sputtering yield Y of organic and inorganic materials bombarded by argon clusters have been reported and fitted with empirical or phenomenological models.[1,2] The general trend is a linear evolution of Y/n as a function of E/n above a certain value of E/n, say 10 eV, and a nonlinear increase of Y/n below that value, with an energy threshold for the linear evolution varying slightly with sputtered material. With decreasing E/n, the ion yield was reported to decrease faster than the sputtering yield, thus obstructing SIMS analysis with large clusters.[3]

The sputtering induced by argon clusters in organic materials and polymers has also been estimated, using molecular dynamics (MD) simulations of single impacts.[4–8] In particular, the calculated dependences of the scaled sputtering yield (Y/n or Y/m) as a function of the scaled energy (E/n or E/m) turned to be identical to the experimental ones. This behavior of universal curves with a break between a linear and a nonlinear region is not specific to Ar clusters, since it was previously predicted for buckminsterfullerenes,[9] polystyrene clusters[10] and, recently, methane cluster bombardment of organic materials,[8] and also for other materials (solid argon,[11] copper[12]), but with significantly different threshold values for the linear behavior. Attempts to go one step further at rationalizing the universal nature of the sputtering curves by including material properties in the scaling were also performed.[13,14] For the mechanistic explanation of the observed behaviors, the reader is referred to the aforementioned theoretical studies. The relationships between the crater size and the sputtering yield have been less studied[13] and, even though the MD simulation results contain this information, to the best of our knowledge, they have not been discussed at all for organic targets.

In our previous article on argon and methane cluster bombardment of organic solids, the change of the "universal" sputtering curve was demonstrated upon the transition from normal to 45° incidence.[8] In addition, the agreement between the model and the experiments involving similar mass molecules was quantitative for 45° incidence (the common angle in experiments). These results provide us with sufficient confidence to further analyze the microscopic details of the interactions and, in particular, the crater sizes and shapes. In this article, the crater volume is compared to the sputtered volume for organic solids made of 1.4 kDa molecules and a mechanistic explanation is developed. In addition, the case of ultrathin films (2–10 nm) on a hard substrate is explored. It shows that the increase of projectile energy deposited in the organic film after reflection on the substrate induces smaller craters and larger sputtered volumes.

[a]Electronic mail: arnaud.delcorte@uclouvain.be

II. COMPUTER SIMULATIONS

The molecular dynamics simulation program used in this study is the SPUT code developed by the group of B.J. Garrison at Penn State University for sputtering applications.[15] In the classical MD method, Hamilton's equations of motion are numerically integrated over some time interval, providing us with the position and velocity of each particle at each timestep. Forces among the atoms or particles in the system are derived from empirical interaction potentials.

The polymeric target used in this study and the methodology of coarse-graining have been described in detail in previous articles.[16,17] The target was made of united atoms of CH_2 (14 amu) and CH_3 (15 amu) in order to reduce computational expense, for a total polyethylene (PE) chain length of 99 units [formula: CH_3-$(CH_2)_{97}$-CH_3]. The interaction potentials were Lennard–Jones potential functions for PE–PE intermolecular (nonbonding) interactions, and Morse potential functions for the intramolecular (covalent) interactions in the PE chains. Additional details about the sample potential parameters and the making of the samples can be found in Ref. 18. Because of the simplicity of the chosen approach and potentials, the resulting samples should be considered as generic models of amorphous organic samples made of linear macromolecules rather than strictly polyethylene. As in our previous studies, Ar clusters were modeled using Lennard–Jones potentials splined to the KrC repulsive potential at short interdistance.[8] CH_4 clusters were defined at the atomistic level and their interaction modeled using the AIREBO potential for the C–C and C–H interactions, with hydrogen ^{1}H replaced by tritium ^{3}H for computational efficiency.[19] A purely repulsive Molière potential was used to describe the Ar–PE interactions. A weak Lennard–Jones potential, appended to a Molière repulsive wall at short interdistance, was used between the C,H atoms of the projectiles and the CG particles of the PE samples.[8] In all the simulations, the projectile incidence angle was 45°. The trajectories were run for a minimum of 25 ps, up to saturation of the sputtered flux.

Full sets of simulations using Ar_n and $(CH_4)_n$ clusters with energies between 2.5 and 15 keV were conducted using a 1.5 nm-thick damping zone at the bottom and on the four lateral sides of the sample (Langevin algorithm with a friction coefficient), in order to absorb the pressure waves and mimic a semi-infinite, bulk sample. In a second series of simulations, the top layer of the organic sample, with a total thickness d, was left free to move. In contrast, the bottom layer of the sample was fixed by constraining the atoms to their initial positions. The thickness of the fixed layer was adjusted to obtain a free PE film thickness d ranging between 2 and 15 nm. For these samples, damping zones were used for the four lateral sides of the box, but not at the bottom. This arrangement models a thin film of thickness d on an infinitely hard substrate. This case is of course not fully realistic, since substrates with an infinite hardness or stiffness do not exist, but with respect to the impact of large Ar clusters, it constitutes an extreme case that is not so far from the reality of an organic layer on a silicon or a metal substrate, and therefore, provides us with useful qualitative trends. Two different impact points of 10 keV Ar_{3000} were calculated for each value of d.

III. RESULTS AND DISCUSSION

A. Semi-infinite organic solid

In our simulations of argon and methane cluster bombardment of amorphous polymeric solids, all the crater shapes can be reasonably approximated by semiellipsoids, with z, the crater depth being the vertical semiaxis and x, y being, respectively, the lengths of the horizontal principal axis in the direction of the beam and of the transverse principal axis, as shown in the inset of Fig. 1(a). With these definitions, Fig. 1 reports the depths and the lateral dimensions of the craters induced by Ar and CH_4 clusters (45° incidence) as a function of cluster size n. It is apparent that the crater depth is proportional to the total kinetic energy of a cluster but varies little with the cluster size, with no obvious trend for both projectile types. In contrast, the lateral dimensions of the craters increase remarkably with cluster size in both cases—from 120 to 215 Å at 10 keV between $(CH_4)_{30}$ and $(CH_4)_{8391}$. Another striking feature is the very similar values of the ellipsoid x and y axis lengths, over the tested range of cluster sizes and energies, except for 15 keV $(CH_4)_n$ bombardment. However, our past simulations showed that 15 keV should be an upper limit of energy for the size of our system and slight edge effects cannot be totally discarded there. At each energy, there is a certain cluster size, for which the lateral dimensions are almost exactly twice the crater depth, meaning that the crater is semispherical. This cluster size n is in the range 30–300 for $(CH_4)_n$ at 2.5 keV and increases to values in the range 1000–5000 at 10 keV. Similar observations can be drawn for Ar_n clusters. This means that the ellipsoids tend to be slightly elongated toward the depth for smaller clusters and rather flattened for larger clusters, with a crossing point varying with the cluster energy. Finally, the craters are generally smaller for $(CH_4)_n$ clusters than for Ar_n clusters at the same energy and cluster size. All these results suggest that the crater size and shape are a complex function of the cluster nature, energy and nuclearity (not mentioning the incidence angle which is constant in our simulations).

These different dependencies, however, resolve into a single curve for each cluster type when the crater volume V is scaled by the cluster nuclearity n or the cluster mass m and plotted versus the cluster energy, which in turn is scaled in the same manner [Fig. 2(a)]. The cluster mass was selected for the scaling, in order to retain consistency with our previous article, where the sputtering yields were discussed for the same system.[8] The evolutions shown by the log-log plot of Fig. 2(a) tend to be linear at high energy, but are clearly sublinear at low energy, with a smooth transition that spans over a wide range of energies. This plot should be compared to the one of the sputtering yields in Ref. 8. It is apparent from the different evolutions of the curves of Y/m and V/m that the ratio between the sputtered volume and the crater volume should not be constant over the investigated range of

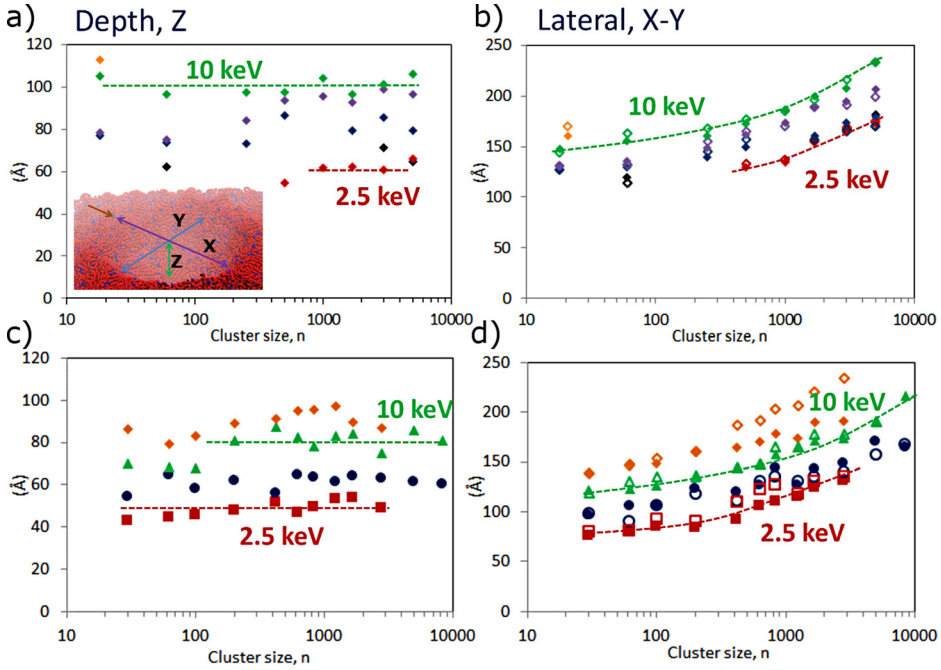

FIG. 1. (Color online) Crater depth z [(a), (c)] and lateral dimensions x, y [(b), (d)] as a function of cluster size n and energy E for Ar_n [(a), (b)] and $(CH_4)_n$ [(c), (d)] cluster bombardment of a CH_3-$(CH_2)_{97}$-CH_3 solid.

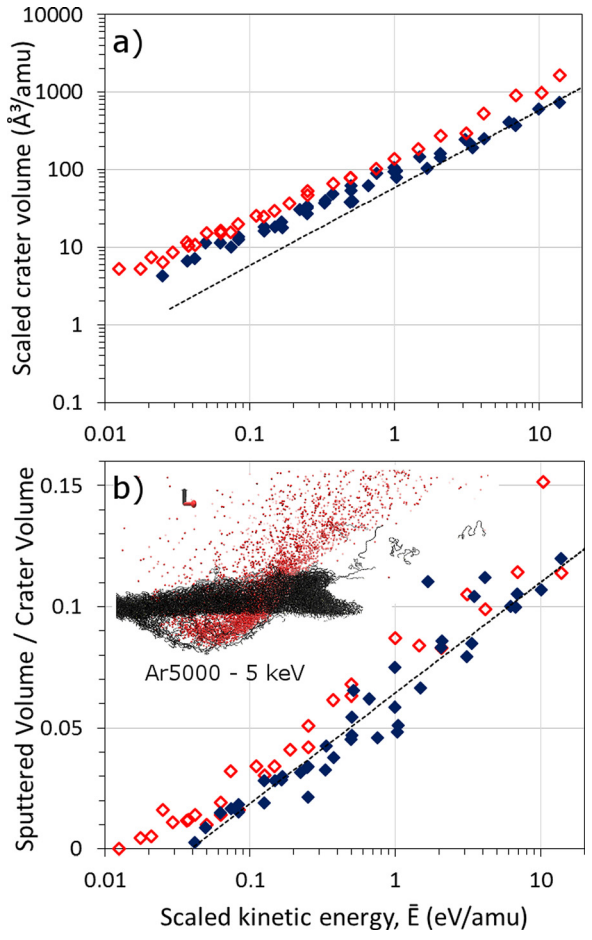

FIG. 2. (Color online) (a) Calculated scaled crater volumes V/m as a function of scaled energy E/m for a CH_3-$(CH_2)_{97}$-CH_3 solid bombarded by Ar_n and $(CH_4)_n$ clusters. (b) Ratio of the sputtered yield volume Y_v to the crater volume V as a function of scaled energy E/m. *Inset:* snapshot of the MD showing the impact of 5 keV Ar_{5000}.

E/n. The ratio of the sputtered yield volume, Y_v, derived from the sputtered masses and the density of our material, to the crater volume, V, is shown in Fig. 2(b). The ratio Y_v/V increases monotonically from 0 to 0.12 over the computed range of scaled energies. These values may seem very small, because they mean that a maximum of 10%–15% of the volume of the crater is actually sputtered as a result of the cluster impact. They can be qualitatively explained by the observation that (1) a very pronounced rim is formed around the craters and (2) many polymeric chains remain dangling above the surface without being ejected [inset of Fig. 2(a) and Ref. 8]. It should be noted that the plot of Fig. 2(b) is semilogarithmic; therefore, the rate of increase of the ratio Y_v/V becomes smaller and smaller as E/n increases.

The observed behavior can be tentatively explained by the different energy deposition in the solid for different values of E/m. Figure 3 shows the time-evolution of the kinetic energy of the projectile and the kinetic energy deposited in different layers (4 nm thickness each) of the surface over the first 6 ps of the interaction. At high E/m [1 eV/amu, Fig. 3(a)], almost all the projectile kinetic energy is deposited in the solid, with a large peak in the first ps in the topmost layers (see the red curve corresponding to energy deposition in the top 4 nm). At low E/m [0.05 eV/amu, Fig. 3(b)], more energy is backscattered with the projectile atoms and the kinetic energy peak in the topmost layer disappears. This change of energy deposition in the top 4 nm of the solid could be directly correlated to the sputtered mass in Ref. 8. The interaction gradually evolves from a situation where a significant fraction of energy is used for sputtering at high E/m to a situation where the energy deposited in the solid is essentially used for material deformation at low E/m. This shift also explains the lateral size of the craters increasing

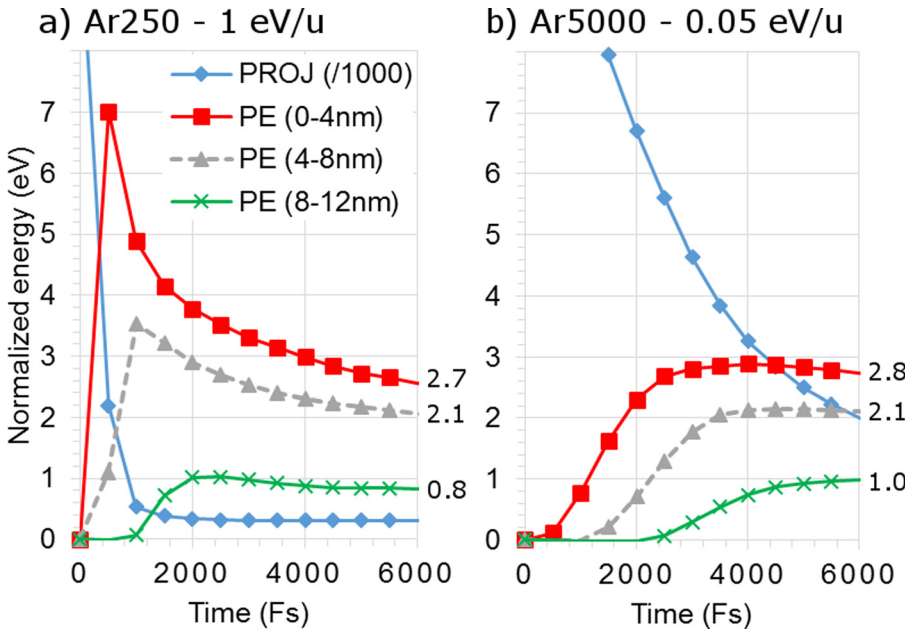

FIG. 3. (Color online) Time-evolution of the kinetic energy of impinging Ar_n clusters (PROJ—divided by 1000) and of the kinetic energy deposited at different depths in the bombarded CH_3-$(CH_2)_{97}$-CH_3 (PE) solid. (Normalized energy: the total kinetic energy is divided by the number of molecules in the considered layer.) The initial kinetic energy of the projectiles is 10 keV. (a) Ar_{250}, 45° incidence (1.0 eV/amu); (b) Ar_{5000}, 45° incidence (0.05 eV/amu).

with n for a given energy in Fig. 1. At constant total kinetic energy, more deformation is caused in the solid with larger clusters (low E/m). In parallel, the sputtered material originates from the top third of the crater at high E/m, and becomes gradually limited to surface molecules at low E/m. This observation indicates that large, slow clusters should provide more surface sensitivity for cluster-based analysis.[8]

B. Ultrathin organic layer

As explained in the Sec. II, thin layers on a hard substrate were modeled by freezing the substrate atoms below a certain depth d. The horizontal friction zone used to absorb the pressure waves at the bottom of the simulation cell (in order to mimic a semi-infinite organic solid) was also removed, so that the deposited energy encounters a reflective wall when reaching depth d. In Fig. 4, the calculated sputtered masses are plotted as a function of d (from 2 to 14.5 nm) for 10 keV Ar_{3000} bombardment. The values arbitrarily plotted at 20 nm correspond to the semi-infinite sample of section A, with a horizontal friction zone at the bottom. Figure 4 shows that the sputtered mass remains close to 4×10^4 amu in the range of the semi-infinite solid down to 7.5 nm films. For films thinner than 7.5 nm, the sputtered mass increases drastically, with a maximum for $d = 4$ nm, then decreases toward lower values of d. The variation of the sputtered mass for two different impact points gives an idea of the scattering of the data at each thickness. The obvious interpretation of the sputtered mass increase for ultrathin layers is related to the confinement of the projectile energy in a polymer layer becoming thinner and thinner. The decrease observed for $d < 4$ nm can be attributed to the decreasing quantity of material available for sputtering.[20] It is probably not a coincidence that 4 nm is also the layer thickness where energy deposition is the most efficient for sputtering, as noted above and in Ref. 8.

Figure 5 shows snapshots of the molecular dynamics for a sample with $d = 10$ nm [(a)–(c)] and a sample where $d = 4$ nm [(d)–(f)]. In the former case the sputtering yield is already in the "bulk" regime, and in the latter case the sputtering yield is at maximum. The crater shapes are no longer spherical, even for $d = 10$ nm (in Fig. 1, 10 keV Ar_{3000} creates an almost hemispherical crater with depth $z = 10$ nm). Both crater shapes here are clearly affected by the confinement of the organic layer. In particular, the crater computed for $d = 4$ nm is wider and has a flat bottom at $z = 4$ nm, as it should be. At the same time the total crater volume V decreases slightly when going from $d = 10$ nm to $d = 4$ nm.

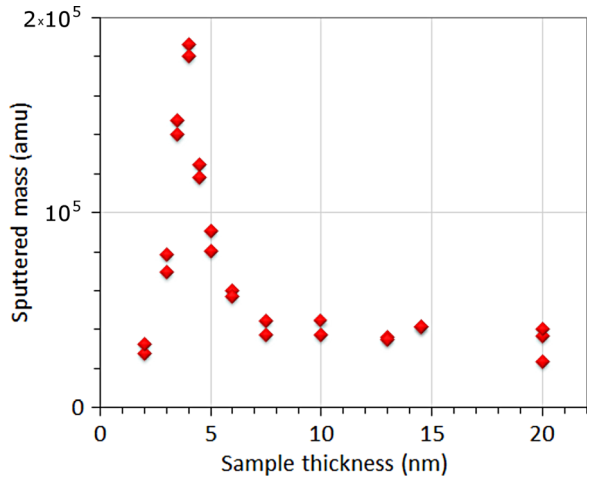

FIG. 4. (Color online) Sputtered mass as a function of layer thickness d for ultrathin films of CH_3-$(CH_2)_{97}$-CH_3 on a rigid substrate (10 keV Ar_{3000} bombardment).

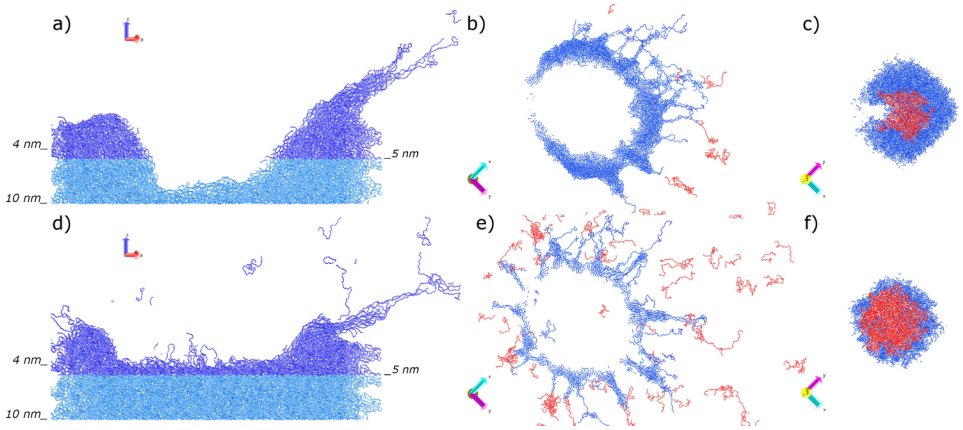

FIG. 5. (Color online) Craters formed by 10 keV Ar_{3000} in ultrathin CH_3-$(CH_2)_{97}$-CH_3 films with a thickness $d = 10$ nm [(a)–(c)] and $d = 4$ nm [(d)–(f)]. [(a), (d)] Cross-sections—The top 5 nm are in dark blue and the bottom 5 nm in light blue; [(b), (e)] material above the surface at 25 ps: ejected in red and attached to the surface in blue; [(c), (f)] the same material relocated to its original position in the surface before the impact.

However, an interesting difference between these 2 cases appears when looking at the material that is above the initial sample surface at the end of the calculation (the rim and sputtered particles). For $d = 10$ nm, the quantity of sputtered material (red) is small while the amount of material forming the crater rim and the dangling chains attached to it (blue) is huge.

In contrast, for $d = 4$ nm, a much larger fraction of the molecules above the surface are sputtered and the remaining rim material is significantly reduced. This is even more obvious when the sputtered and rim material is traced back to its original position in the solid at t = 0 ps [Figs. 5(c) and 5(f)]. This example demonstrates that the ratio between sputtered volume Y_v and crater volume V is much higher for ultrathin films on a hard substrate than for bulk organic samples.

IV. CONCLUSIONS

In this article, the dependences of the impact crater volumes on energy E and nuclearity n were obtained by MD computation for organic samples bombarded by $Ar_{18\text{-}5000}$ and $(CH_4)_{30\text{-}8391}$ projectiles. Although the crater sizes and shapes depend on both parameters (E,n), the different evolutions can be reshaped into one universal curve if energies and volumes are scaled to the projectile mass m or nuclearity, in a manner similar to the sputtering yields. The ratio of the sputtering yield to the crater volume decreases when E/m decreases, so that slow and large clusters cause extensive deformation and molecular displacement on the sample surface with minimal sputtering. At the same time, the sputtered molecules are essentially intact and originate in the topmost surface layer. The ratio between sputtering yield and crater size increases strongly when going from thick organic films to thin layers (2–7 nm) on a hard substrate, because of the energy confinement in the molecular layer. In those nanometer-thick layers, sputtering is comparatively more efficient. This effect was recently confirmed by carefully designed experiments with ultrathin polymeric layers.[21]

ACKNOWLEDGMENT

A.D. is a research director of the Belgian "Fonds National de la Recherche Scientifique."

[1] M. P. Seah, J. Phys. Chem. C **117**, 12622 (2013).
[2] P. J. Cumpson, J. F. Portoles, A. J. Barlow, and N. Sano, J. Appl. Phys. **114**, 124313 (2013).
[3] S. Rabbani, A. M. Barber, J. S. Fletcher, N. P. Lockyer, and J. C. Vickerman, Anal. Chem. **83**, 3793 (2011).
[4] O. A. Restrepo and A. Delcorte, J. Phys. Chem. C **117**, 1189 (2013).
[5] Z. Postawa, R. Paruch, L. Rzeznik, and B. J. Garrison, Surf. Interface Anal. **45**, 35 (2013).
[6] A. Delcorte, V. Cristaudo, V. Lebec, and B. Czerwinski, Int. J. Mass Spectrom. **370**, 29 (2014).
[7] Z. Postawa, M. Kanski, D. Maciazek, R. J. Paruch, and B. J. Garrison, Surf. Interface Anal. **46**, 3 (2014).
[8] A. Delcorte and M. Debongnie, J. Phys. Chem. C **119**, 25868 (2015).
[9] K. E. Ryan and B. J. Garrison, Anal. Chem. **80**, 6666 (2008).
[10] A. Delcorte, B. J. Garrison, and K. Hamraoui, Anal. Chem. **81**, 6676 (2009).
[11] C. Anders, H. M. Urbassek, and R. E. Johnson, Phys. Rev. B **70**, 155404 (2004).
[12] C. Anders and H. M. Urbassek, Nucl. Instrum. Methods Phys. Res. B **315**, 304 (2013).
[13] C. Anders, E. M. Bringa, F. D. Fioretti, G. Ziegenhain, and H. M. Urbassek, Phys. Rev. B **85**, 235440 (2012).
[14] R. J. Paruch, Z. Postawa, and B. J. Garrison, Acc. Chem. Res. **48**, 2529 (2015).
[15] B. J. Garrison, A. Delcorte, and K. D. Krantzman, Acc. Chem. Res. **33**, 69 (2000).
[16] E. J. Smiley, Z. Postawa, I. A. Wojciechowski, N. Winograd, and B. J. Garrison, Appl. Surf. Sci. **252**, 6436 (2006).
[17] A. Delcorte and B. J. Garrison, J. Phys. Chem. C. **111**, 15312 (2007).
[18] K. Hamraoui and A. Delcorte, J. Phys. Chem. C **114**, 5458 (2010).
[19] S. J. Stuart, A. B. Tutein, and J. A. Harrison, J. Chem. Phys. **112**, 6472 (2000).
[20] L. Rzeznik, R. Paruch, B. Czerwinski, B. J. Garrison, and Z. Postawa, Vacuum **83**, S155 (2009).
[21] V. Cristaudo, C. Poleunis, and A. Delcorte, "Effect of nanoconfinement on the sputter yield in ultrathin polymeric films: Experiments and model," Appl. Surf. Sci. (in press).